Electrochemical Tuning of Electronic Structure of Single-Walled Carbon Nanotubes: In-situ Raman and Vis-NIR Study

Ladislav Kavan,*,†,‡ Peter Rapta,†,§ Lothar Dunsch,† Michael J. Bronikowski,||,⊥ Peter Willis,|| and Richard E. Smalley||

Institute of Solid State and Materials Research, Helmholtzstrasse 20, D-01069 Dresden, J. Heyrovský Institute of Physical Chemistry, Academy of Sciences of the Czech Republic, Dolejškova 3, CZ-182 23 Prague 8, Slovak University of Technology, Radlinského 9, SK-812 37 Bratislava, and The Center for Nanoscale Science and Technology, Rice University, MS 60, 6100 Main St., Houston, Texas 77005-1892

Received: May 4, 2001; In Final Form: August 13, 2001

The population of valence-band electronic states of single-walled carbon nanotubes (SWCNTs) was tuned electrochemically in acetonitrile electrolyte solution. In dry and oxygen-free solution, the electrochemistry of SWCNTs is controlled by capacitive charging. Reversible changes of intensity and frequency of the Raman spectra can be monitored during cyclic voltammetry at low scan rates. Electrochemical charging of SWCNTs can be also traced via reversible bleaching of the electronic transitions in the vis-NIR region. An aprotic medium offers a broader electrochemical window for tuning of electronic properties of SWCNTs. Electrochemical charging of SWCNTs in an aprotic electrolyte solution allows easy and precise control of the electronic structure of SWCNTs. In addition to commercial SWCNTs, a material made from gas-phase catalytic decomposition of CO by the HiPco process was also studied. Selective quenching of vis-NIR and Raman spectra is a useful tool to the analysis of tubes of varying diameter and helicity.

1. Introduction

Studies of electron transfer processes on single-walled carbon nanotubes (SWCNTs) have focused on practical issues of hydrogen storage,[1,2] Li batteries,[3] and supercapacitors.[4−8] The electrochemical hydrogen storage capacities were reported to be 110 mAh/g (0.39 wt % H_2)[2] or 800 mAh/g (2.9 wt %).[1] These values are still somewhat smaller than those observed for the sorption from the gas phase, 4.2 wt %.[9] Lithium insertion into SWCNTs is characterized by larger capacity compared to that of graphite (372 mAh/g for LiC_6), faster kinetics, and absence of staging.[3] Since the intercalation between graphene layers is ruled out in SWCNTs, lithium is, presumably, accommodated in nanochannels occurring inside the nanotube bundles and ropes.[3] Carbon nanotubes are competitive to activated carbon for supercapacitors, as they typically achieve capacitances of ca. 15−100 F/g,[4−6,8,10,11] but even higher values (283 F/g) were also reported.[7]

The Raman and vis-NIR spectra of SWCNTs are understood in terms of resonance enhancement and optical band-gap excitation in a one-dimensional conductor with Van Hove singularities in the electronic density of states.[12−16] Chemical redox processes can modify the population of such states. Reduction of SWCNTs by alkali metals[17,18] and anion radicals[16,19] and oxidation with Br_2 and I_2 [16−18] were followed by Raman,[17,20] vis-NIR,[15,16,18] and resistivity measurements.[15,18] The most characteristic issue is bleaching of optical transitions associated with amphoteric depleting or filling of the corresponding electronic states via chemical doping of SWCNTs.[15−17,19]

The electronic structure of SWCNTs can be tuned by chemical doping with molecules possessing different redox potentials.[16,19] Alternatively, the electronic structure can be changed electrochemically by controlling the interfacial potential of SWCNTs in contact with an electrolyte solution. The electrochemical tuning is apparently more easy and more precise compared to chemical doping. We have recently presented a first study of SWCNTs employing in-situ Raman and vis-NIR spectroelectrochemistry in an aqueous electrolyte solution.[12] The aim of this paper is to upgrade these studies by the application of nonaqueous media and by exploring the behavior of tubes of different diameters and chirality.

2. Experimental Section

The purified SWCNT material was purchased from Tubes@Rice (sample No. P06049-6, suspended in toluene). This material is further referred to as TR-SWCNT. Besides TR-SWCNT, nanotubes were also prepared via iron-catalyzed decomposition of carbon monooxide by the HiPco process.[21,22] These tubes are further referred to as CO-SWCNT. The electrolyte solution was 0.2 M $LiClO_4$ in acetonitrile (both from Aldrich) dried by 4A molecular sieves. The water content in the electrolyte solution was ∼10 ppm (Karl Fischer titration, WTK 891 coulometer, Diram, CZ). Electrochemical experiments were carried out using HEKA IEEE-488 or EG&G PAR 273A potentiostats, with Pt auxiliary and Ag/AgCl (saturated LiCl) reference electrodes. The electrochemical cell was equipped with standard screw joints for the electrodes, sealed with Viton O-rings and Teflon gaskets. The electrolyte solution was purged with nitrogen, and the cell was assembled under nitrogen atmosphere in a glovebox (M. Braun GmbH, the box atmosphere contained typically <1 ppm of O_2 and H_2O). The working electrode was a thin film of SWCNT deposited on Pt, Au, or ITO (indium−tin oxide conducting glass). A thin film of

* Corresponding author. Fax: +420-2-86582307; e-mail: kavan@jh-inst.cas.cz.
† Institute of Solid State and Materials Research.
‡ J. Heyrovský Institute of Physical Chemistry.
§ Slovak University of Technology.
|| Rice University.
⊥ Present address: Jet Propulsion Laboratory, 4800 Oak Grove Drive, Pasadena, CA, 91109-8099.

10.1021/jp011709a CCC: $20.00
Published on Web 10/16/2001

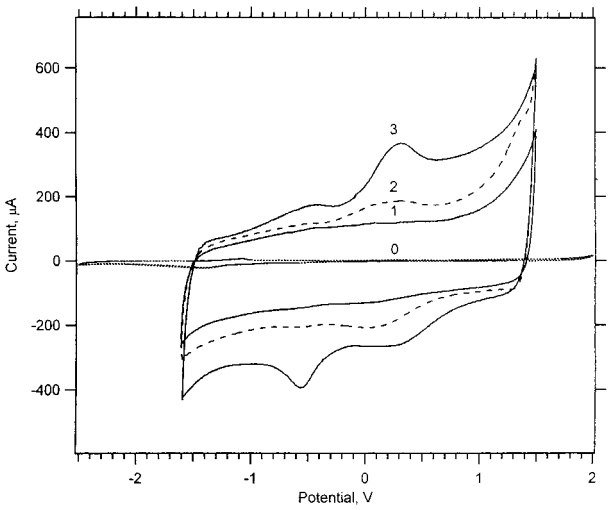

Figure 1. TR-SWCNT: Cyclic voltammogram on Pt electrode in 0.2 M $LiClO_4$ + acetonitrile (water content 10 ppm), scan rate 0.1 V/s. (Curve 0) Blank Pt electrode. (Curve 1) Freshly assembled cell measured in a drybox. (Curves 2 and 3) The closed cell removed from a drybox and exposed to air for 1 day (2) or 3 days (3). TR-SWCNT weight 0.036 mg.

nanotubes was deposited by spraying a freshly sonicated methanol−toluene (3:1 v/v) suspension of SWCNTs on an electrode surface heated with hot air. The film was outgassed at 100−150 °C in a vacuum and further handled in a glovebox under nitrogen. The film mass was typically between 0.01 and 0.06 mg. For more precise electrochemical studies, the SWCNT film was deposited on gold film supported by quartz crystal (1000 Å of Au on 100 Å of Cr; AT cut 10-MHz quartz crystals, International Crystal Manufacturing Company, Oklahoma), and the mass was measured by a quartz microbalance (EQCM-5510, PAS, Poland).

For in-situ Raman measurements, the cell was equipped with a glass optical window. Raman spectra were excited by an Ar^+ laser, $\lambda = 514.5$ nm, 25 mW (Innova 305, Coherent) or by a Ti-saphire laser, $\lambda = 754.0$ nm, 3 mW (899LC, Coherent). The spectra were recorded on a T-64000 spectrometer (Instruments, SA) interfaced to an Olympus BH2 microscope. The spectrometer was calibrated before each series of measurements by using the F_{1g} mode of Si at 520.2 cm^{-1}. A second calibration was carried out by using the Raman bands of acetonitrile as an internal standard (vide infra).

The ITO-supported SWCNTs served for in-situ vis-NIR spectroelectrochemistry in 0.2 M $LiClO_4$ + acetonitrile. The spectra were recorded on a double-beam Shimadzu 3100 spectrometer. The working electrode was placed in a 1-mm optical cell with Pt auxiliary and Ag/AgCl reference electrodes. Optical densities were normalized against a second optical cell with a blank ITO electrode.

3. Results and Discussion

3.1. Cyclic Voltammetry. Figure 1 displays typical cyclic voltammograms of TR-SWCNTs in 0.2 M $LiClO_4$ + acetonitrile. The voltammogram in a freshly assembled and hermetically closed cell (curve 1) displays a monotonic charge injection over the whole potential range. The specific capacitance, C, can be calculated from the current, I, at the given scan rate, υ, and weight of the SWCNT layer, m:

$$C = I/\upsilon m, \tag{1}$$

which gives ca. 40 F/g for the electrode in Figure 1 (curve 1) between the potentials of −0.5 to 0.5 V. In this region, the SWCNT approaches the behavior of an ideal double-layer capacitor. The found capacitance is comparable to that observed in aqueous medium (25−75 F/g),[12] but our value is apparently lower than the capacitance of SCWCNT in acetonitrile electrolyte solution reported by some other authors.[7] The voltammogram changes if the cell is stored for days in air atmosphere (curves 2, 3). This is presumably caused by penetration of oxygen and humidity into the electrolyte solution. The peaks observed at curves 2 and 3 are presumably due to faradaic pseudocapacitance associated with oxygen-containing surface functionalities on SWCNTs and/or on carbonaceous impurities in the sample. In aqueous media, the charging of surface oxides on SWCNTs and/or carbons was found to be pH dependent, which can be schematically represented by a generic expression[5]

$$\text{=C=O} + \text{H}^+ + \text{e}^- \rightleftarrows \text{=COH} \tag{2}$$

Baughman et al.[10,11] have observed a distinct voltammetric peak of SWCNT in $LiClO_4$ + acetonitrile. They have assigned the cathodic peak ca. −0.6 V to −0.7 V (vs Ag/Ag^+) to the insertion of Li^+ into the interstitial region in nanotube bundles. In contrast to that, Smalley et al.[3] observed a featureless voltammogram in dry $LiPF_6$ + dimethyl carbonate + ethyl carbonate (3 ppm H_2O); Li insertion was traced only by the monotonic rise of cathodic current at very low potentials (0.5 to 0 V vs Li/Li^+). We assign the voltammetric peaks in Figure 1 (curves 2 and 3) to faradaic pseudocapacitance (eq 2), which is promoted by trace humidity in the acetonitrile medium. Another argument for our interpretation is the fact that the peak currents (in Figure 1, curves 2 and 3) were found to be proportional to the scan rate. This speaks for surface charging (eq 2) but rules out a diffusion-controlled process ($I \approx \upsilon^{1/2}$), which one would expect for Li^+ insertion.

3.2. Vis-NIR Spectroscopy. The open-circuit potential (OCV) of a SWCNT electrode in 0.2 M $LiClO_4$ + acetonitrile is usually between 0 to −0.2 V. At potentials close to OCV, the vis-NIR of ITO-supported TR-SWCNT show three characteristic optical absorptions at 0.75, 1.3, and 1.9 eV, which can be attributed to the optical transitions between Van Hove singularities of the density of electronic states of SWCNTs (Figure 2, upper plot). The first two transitions are assigned to semiconducting tubes ($\upsilon_s^1 \rightarrow c_s^1$) and ($\upsilon_s^2 \rightarrow c_s^2$), respectively, whereas the feature at 1.9 eV corresponds to the first pair of singularities in metallic tubes ($\upsilon_m^1 \rightarrow c_m^1$).[13,14,16,18,23] These bands are actually overlapping features of individual tubes distinguished by their dimensions and helicity. The CO-SWCNTs show more complex vis-NIR spectra (Figure 2, lower plot), but the principal transitions, ($\upsilon_s^1 \rightarrow c_s^1$) and ($\upsilon_s^2 \rightarrow c_s^2$), can still be traced at ca. 1 and 2 eV, respectively. Since the transition energies are known to scale with tube diameter,[13,14,16,18] we can estimate the corresponding diameters of semiconducting tubes to be about 1.2 nm or (0.8−0.9) nm for TR-SWCNTs or CO-SWCNTs, respectively. The detailed plots of the $\upsilon_s^1 \rightarrow c_s^1$ transition in TR-SWCNTs and CO-SWCNTs (Figure 3) show that the narrow semiconducting tubes in CO-SWCNTs are rather polydisperse, exhibiting four distinct maxima of tubes distributed between ca. 0.8 to 0.9 nm.

Electrochemical charging of SWCNTs causes reversible bleaching of these transitions, which is in accord with previous reports employing chemical[15,16,18,24] and electrochemical[12,24] redox doping. Anodic polarization shifts the Fermi level, while the corresponding singularities are depleted in the sequence c_s^1, c_s^2, c_m^1. Analogously, cathodic polarization leads to sequential filling of the singularities: υ_s^1, υ_s^2, υ_m^1. In both cases, the optical absorption bands should disappear in the same sequence, i.e.,

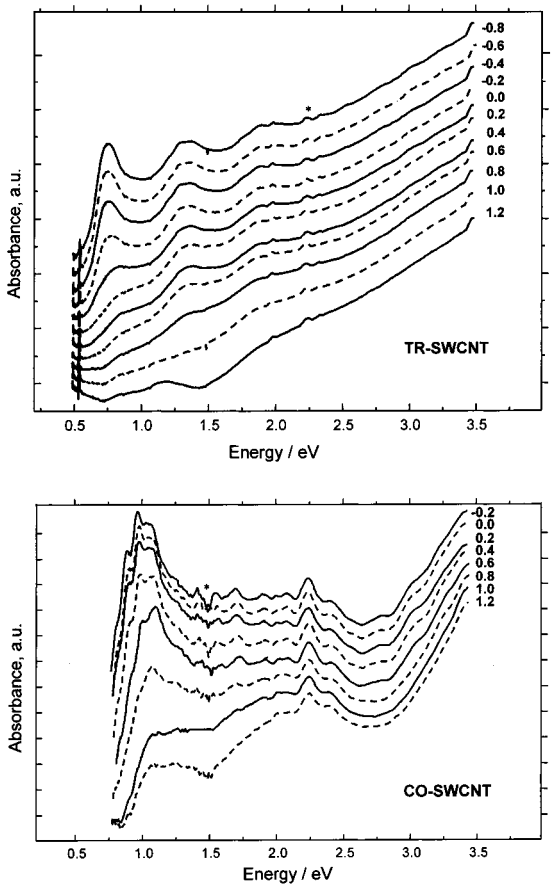

Figure 2. Vis-NIR spectra of ITO-supported nanotube film in 0.2 M $LiClO_4$ + acetonitrile. The applied potential (in V vs Ag-reference electrode) is labeled on each curve. Asterisk (*) denotes an artifact introduced by the used spectrometer.

in the series of increasing gap energies. The bleaching of the first transition ($\upsilon_s^1 \rightarrow c_s^1$) can be detected even in an aqueous electrolyte solution, but higher gap energies are poorly accessible owing to the limited potential window.[12] Further depletion/filling of electronic states is possible only in a nonaqueous medium.[24]

At deeper doping in acetonitrile medium, we can trace two new effects that were not detectable in aqueous medium.[12] (i) The maximum of electronic transitions shifts to higher energies (cf. Figures 2 and 3), as it is expected from the energy vs diameter dependence:[13,14] the corresponding states of wide tubes are depleted/filled at lower potentials than the same states of narrow tubes. (ii) At very high potentials (≈1.2 V), we can even trace new transition in TR-SWCNT at ca. 1.2 eV (Figure 2 upper plot). This "doping induced transition" can be presumably assigned to transitions within the partly filled valence band ($\upsilon_s^n \rightarrow \upsilon_s^1$, $\upsilon_s^n \rightarrow \upsilon_s^2$) $n \geq 3$).[15,18]

Bleaching of electronic transitions at several selected photon energies is further illustrated in Figure 4. Each curve was normalized assigning absorbances 0/1 to the minimum/maximum values, respectively at the given potential excursion (−0.2 to 1.2V). The plot in Figure 4 was essentially mirrored also during the cathodic potential excursion. However, the optical measurements at deep cathodic potentials are complicated by inherent instability of the supporting material (ITO) toward cathodic breakdown, especially in less dry electrolyte solutions. (At the anodic side, the ITO electrode is perfectly stable, even in aqueous medium.[12])

Figure 5 shows the absorbance at 0.75 eV of the TR-SWCNT electrode, which was polarized by square-wave potential pulses.

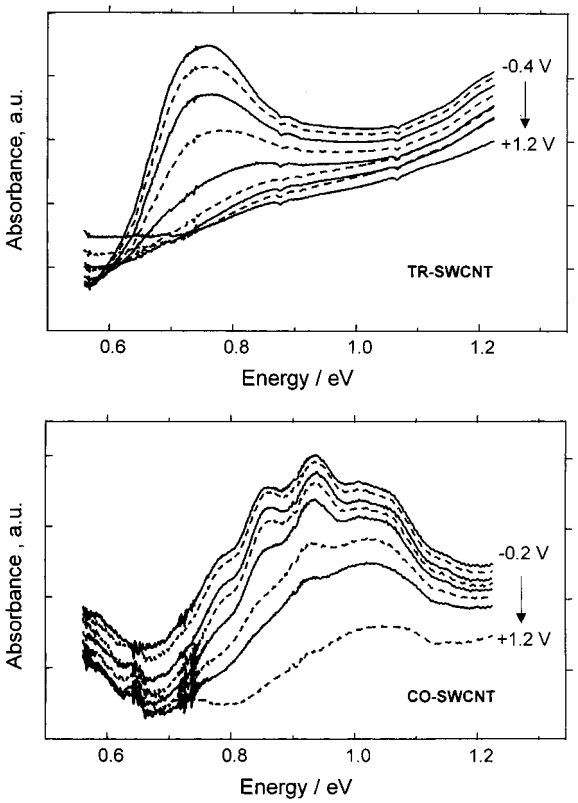

Figure 3. NIR spectra of ITO-supported nanotube film in 0.2 M $LiClO_4$ + acetonitrile. The applied potential varied by 0.2 V from −0.4 V or −0.2 V (top curve) to 1.2 V (bottom curve).

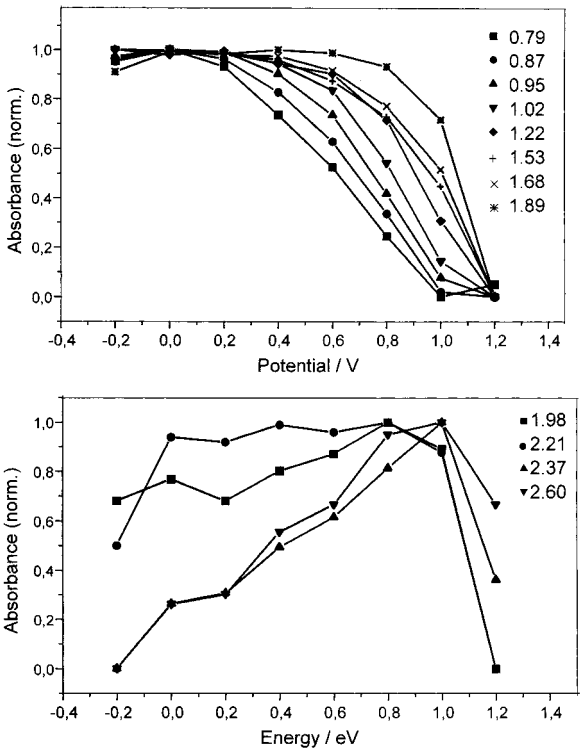

Figure 4. Normalized optical absorbance of CO-SWCNTs at various photon energies as a function of potential in 0.2 M $LiClO_4$ + acetonitrile. The photon energy (in eV) is labeled in annotation.

Potentiostatic switching between −0.4 and 1.0 V leads to the corresponding changes in optical density (cf. Figure 3). The absorbance changes are perfectly reversible and occur within the subsecond time domain (Figure 5). This reflects the fact

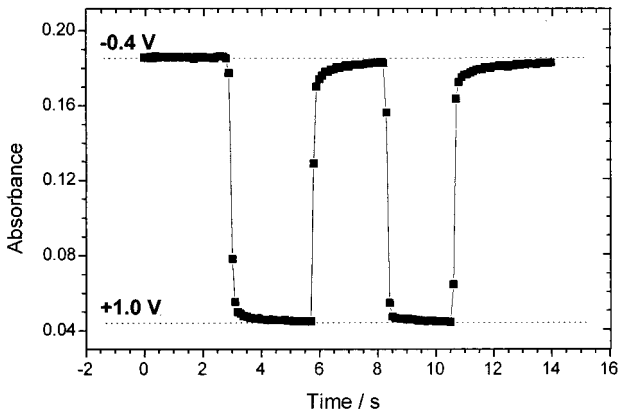

Figure 5. TR-SWCNT: Optical absorbance at 1650 nm (0.75 eV) of ITO-supported TR-SWCNTs in 0.2 M $LiClO_4$ + acetonitrile. The electrode potential was switched between −0.4 V and +1.0 V.

that fast double-layer charging (cf. section 3.1) drives the optical switching. The speed and reversibility compares favorably with that of conventional electrochromic devices, which are usually based on faradaic redox processes.

3.3. Raman Spectroscopy. Figures 6 and 7 show the in-situ Raman spectra of TR-SWCNTs excited at 2.41 eV (Figure 6) and 1.65 eV (Figure 7), respectively. The radial breathing mode (RBM) occurs at about 190 and 210 cm^{-1} (for 2.41 eV excitation, Figure 6) and 175 and 210 cm^{-1} (for 1.65 eV excitation, Figure 7). The diameter of individual SWCNTs (d) in a bundle is known to scale with the RBM frequency (ω):[13]

$$d \approx 232/(\omega\text{-}6.5) \qquad (3)$$

where ω is in cm^{-1} and d is in nm. Equation 3 yields d in the range 1.1 to 1.4 nm for ω between 210 to 175 cm^{-1}, which is in accord with the diameter estimated from vis-NIR spectra (section 3.2). In terms of the zone-folding scheme,[13−15] the excitation energy of 2.41 eV matches the transition ($\upsilon_s^3 \rightarrow c_s^3$) for semiconducting tubes between 1.1 and 1.3 nm (210 to 190 cm^{-1}). The excitation of semiconducting tubes at 2.41 eV is also supported by a narrow and symmetric band of tangential displacement mode (TM) at ca. 1593 cm^{-1}; this band can be fitted to a triplet of Lorentzian lines.[12,13] There is no apparent Raman signal above 220 cm^{-1}, which would account for the resonance of the 2.41 eV-photon with thin metallic tubes (d < 1.1 nm; $\upsilon_m^1 \rightarrow c_m^1$). On the other hand, the $\upsilon_m^1 \rightarrow c_m^1$ transition becomes the dominating resonance for the 1.1−1.4 nm tubes excited at 1.65 eV (Figure 7). Hence, the sample TR-SWCNT is composed from semiconducting tubes (1.1−1.3 nm) and metallic tubes (1.1−1.4 nm).

If the TR-SWCNT electrode is polarized anodically or cathodically (Figures 6 and 7), the main effects are a drop of the Raman intensities of both RBM and TM. Similar behavior was reported for chemical[17] and electrochemical redox doping.[12] In accord with aqueous spectroelectrochemistry,[12] the intensity of the higher frequency RBM of semiconducting tubes (at ca. 210 cm^{-1}) was less affected, compared to the intensity of the main peak at ca. 190 cm^{-1} (Figure 6). This can be easily interpreted, assuming that the anodic or cathodic polarization causes the depletion or filling, respectively, of spikes in the density of electronic states of semiconducting tubes.[12] Since the corresponding transition energies are diameter dependent,[13−15] the υ_s^3/c_s^3 states of wide tubes are depleted/filled first (i.e., before those of narrower tubes), when the potential moves toward more positive/negative values. In other words, narrow tubes persist to be Raman active even at highly negative/positive potentials. Analogously, the band of metallic tubes at 175 cm^{-1} is more sensitive to electrochemical doping than the bands at 190 and 210 cm^{-1} (Figure 7), which again reflects more facile depletion/filling of the υ_m^1/c_m^1 states of wide tubes compared to those of narrow tubes. Qualitatively similar phenomena occur if we slightly decrease the wavelength of the exciting photon: the diameters that can be excited downshift. For instance, narrow semiconducting tubes (ω > 190 cm^{-1}), which are almost idle

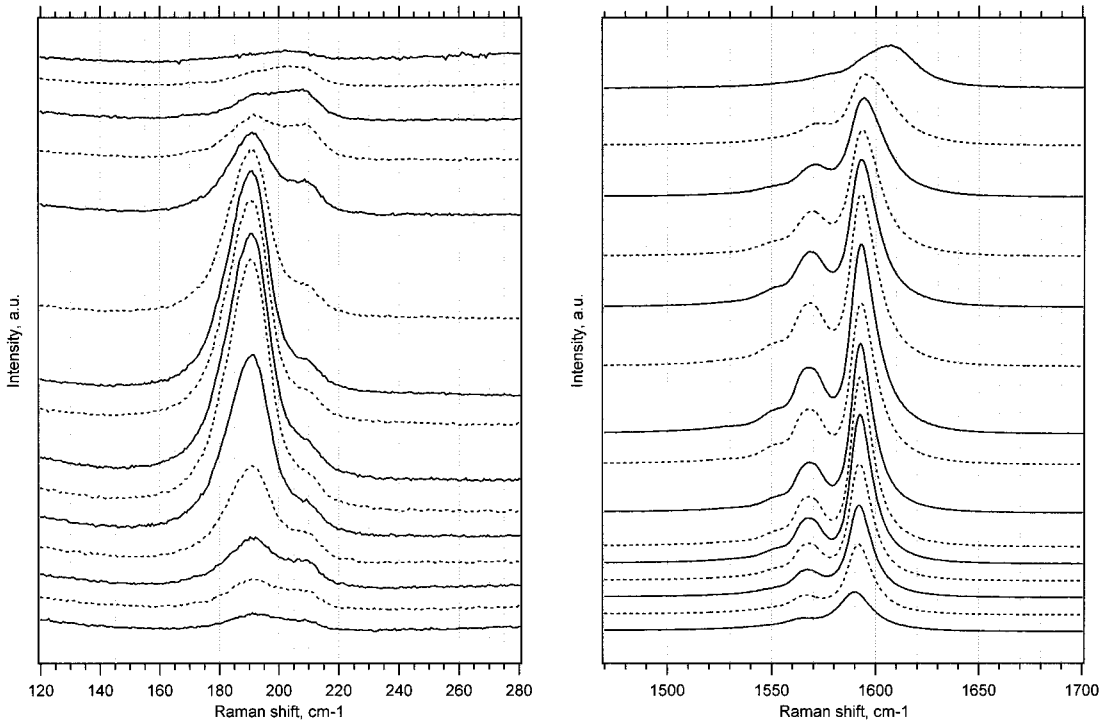

Figure 6. TR-SWCNT: In-situ Raman spectra in 0.2 M $LiClO_4$ + acetonitrile excited at λ = 514.5 nm. The applied potential was (in V vs Ag/AgCl) 1.4, 1.2, 1.0, 0.8, 0.6, 0.4, 0.2, 0, −0.2, −0.4, −0.6, −0.8, −1.0, −1.2, −1.4 for curves from top to bottom. The spectra are offset for clarity, but the intensity scale is identical for all plots in the given spectral region.

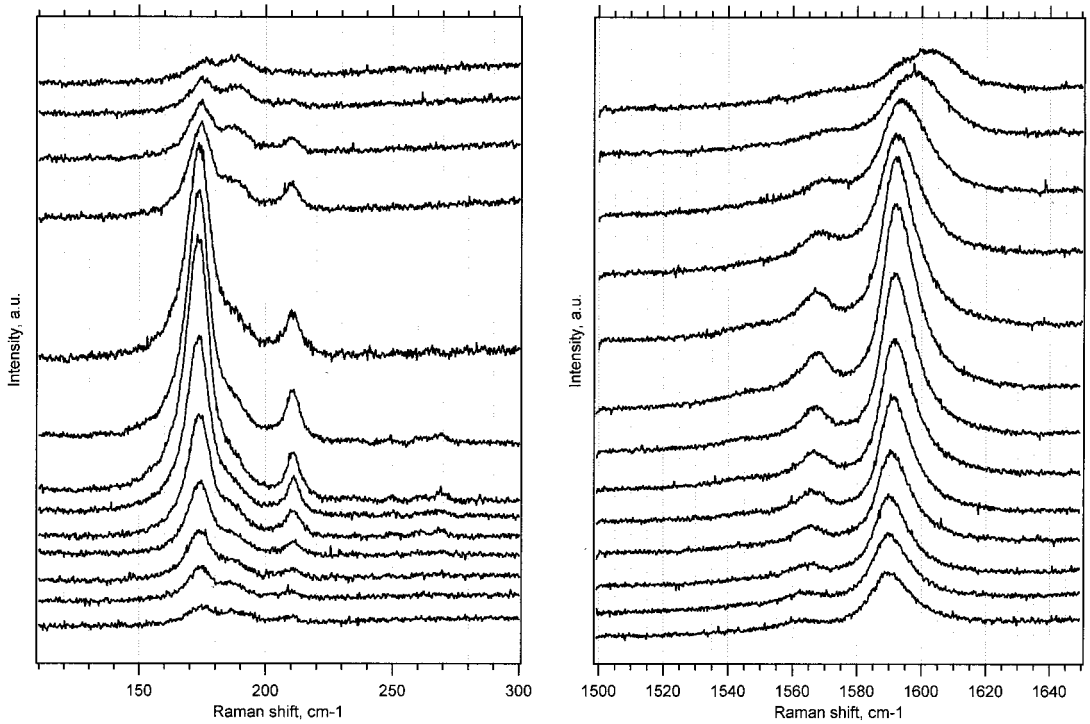

Figure 7. TR-SWCNT: In-situ Raman spectra in 0.2 M $LiClO_4$ + acetonitrile excited at $\lambda = 754.0$ nm. The applied potential was (in V vs Ag/AgCl) 1.2, 1.0, 0.8, 0.6, 0.4, 0.2, 0, −0.2, −0.4, −0.6, −0.8, −1.0, −1.2 for curves from top to bottom. The spectra are offset for clarity, but the intensity scale is identical for all plots in the given spectral region.

at $\lambda = 514.5$ nm, can be resonantly excited at the wavelengths λ from 457 to 496 nm.[13,25] The interband transitions ($\upsilon_s^3 \rightarrow c_s^3$) with energies $\leq$ 2.4 eV are quenched if the potential of a SWCNT electrode shifts by $\geq$1.2 V from the potential of the Fermi level.

Also, the TM band drops along with a small positive/negative shift of the peak position, if the applied potential increases/decreases from OCV. Figure 8 displays the corresponding shifts of intensity and frequency for TR-SWCNTs excited at 514.5 nm. (Analogous dependence was found also for the 754.0 nm excitation.) The TM band of semiconducting TR-SWCNTs (514.5 nm excitation) actually overlaps a multiline feature (two E_g and one A_g modes), but its Lorentzian fitting confirms that all of the individual components exhibit collective frequency shifts.[12,26] The observed shifts can be interpreted as stiffening of the graphene mode if holes are introduced into the π band (anodic polarization) or softening of the graphene mode if electrons are introduced into the π^* band (cathodic polarization).

If we denote the number of electrons transferred per one C atom as f, the $\Delta\omega/\Delta f$ shifts in graphene equal to +460 cm^{-1} for oxidative doping and −140 cm^{-1} for reductive doping, respectively.[17] These values correspond to stage 1 and stage 2 intercalation in graphite, which seems to be a good model of SWCNTs. (For a higher staging index, the graphene may or may not be adjacent to the intercalate, i.e., the Raman spectra show a more complex picture.[27−29])

For an ideal double-layer capacitor (cf. Figure 1, curve 1) we can express

$$\Delta f = M_C C \Delta U / F \qquad (4)$$

where M_C is atomic weight of carbon, ΔU is potential difference, and F is the Faraday constant. Equation 4 yields $\Delta f \approx 0.005 \cdot \Delta U$ for ΔU in V and $C \approx 40$ F/g (see Figure 1 and discussion thereof). Analysis of experimental spectra (as in Figure 6) gives $\Delta\omega/\Delta f = (250 \pm 80)$ cm^{-1} for ΔU between 0.2 and 1.0 V,

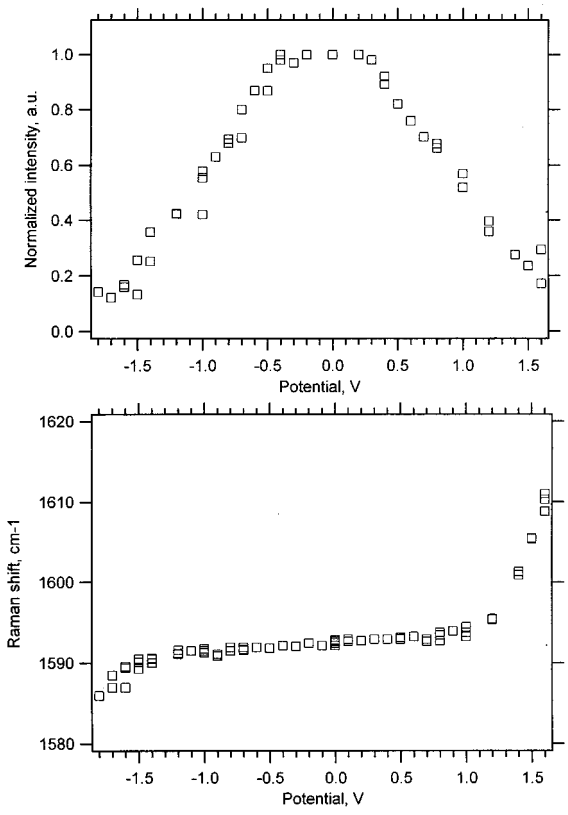

Figure 8. TR-SWCNT: Raman intensity (upper plot) and frequency (lower plot) of the TM band as a function of the applied potential in 0.2 M $LiClO_4$ + acetonitrile. The spectra were excited at $\lambda = 514.5$ nm.

which roughly matches the value of 320 cm^{-1} reported for anodic doping of SWCNTs in H_2SO_4,[26] but our $\Delta\omega/\Delta f$ ratios are much higher than expected for $\Delta U > 1.2$ V. This is apparently caused by irreversible oxidation of SWCNTs.[12,17,26]

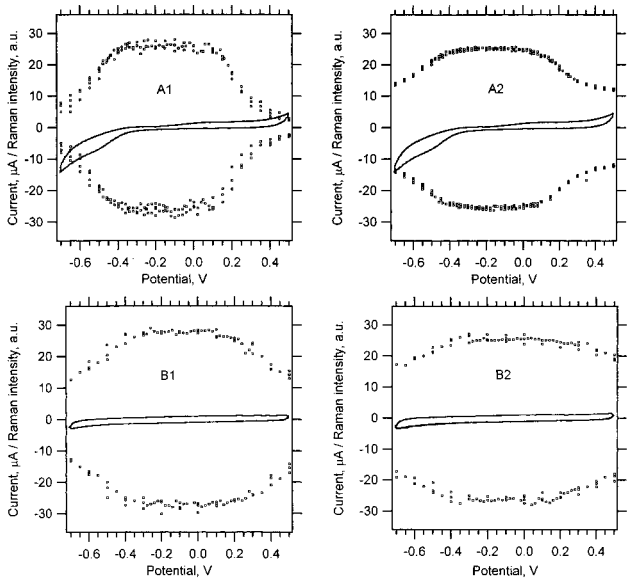

Figure 9. TR-SWCNT: Raman intensity of RBM (A1, B1) and TM (A2, B2) during cyclic voltammetry, scan rate 1 mV/s. The acquisition time for each Raman spectrum was 2 s. A1, A2: electrolyte saturated with air. B1, B2: dry, oxygen-free electrolyte solution.

Irreversible oxidation manifested itself by "burning" of nanotubes after prolonged exposure of anodically polarized SWCNTs to the laser light. At the illuminated site, even a cavity in the SWCNT film can be created. This contrasts to high photochemical and thermal stability of SWCNTs in the dry state. A simultaneous application of the laser light and anodic polarization is essential for the burning of SWCNTs: no breakdown of nanotubes occurred (1) at the areas outside the laser spot of a polarized electrode and (2) by laser excitation of an electrode at less positive potentials.

An analogous evaluation routine for cathodic polarization of TR-SWCNTs yields $\Delta\omega/\Delta f = -(200 \pm 30)$ cm^{-1} for ΔU between -0.2 to -1.2 V. Also in this case, we can detect irreversible reduction below ca. -1.2 V, but the deviation from average $\Delta\omega/\Delta f$ shifts is less dramatic and no "burning" of tubes is apparent at cathodic polarization. Although the experimental errors (in determination of both $\Delta\omega$ and Δf) are high, there is reasonable matching of our values with those previously reported for doping of nanotubes[20,26] and graphite.[17]

Outside the potentials at which the irreversible effects take place, the charge transfer induced shifts are reasonably fast. This reminds of the fast optical switching (Figure 5 and discussion thereof) and even allows recording of Raman spectra during cyclic voltammetry at low scan rates. Figure 9 demonstrates such an experiment at 1 mV/s. The voltammetric currents are mostly capacitive in a dry, oxygen-free electrolyte solution, hence, pseudocapacitance contribution from surface oxides is negligible (cf. section 3.1). The corresponding changes of Raman intensity (Figure 5, curves B1 and B2) seem to be less pronounced, compared to those in air-saturated electrolyte solution (Figure 5, curves A1 and A2).

The CO-SWCNT tubes show a qualitatively similar response to electrochemical polarization (Figures 10 and 11), although the region of RBM exhibits more complex features. Figure 10 evidences a mixture of ≈1.3-nm semiconducting tubes (≈190 cm^{-1}; similar to that in TR-SWCNTs) and narrow tubes with RBM at ca. 250−270 cm^{-1}. In terms of the zone-folding scheme,[13−15] the bands at 250−270 cm^{-1} correspond to resonance on thin metallic tubes ($d < 1$ nm; $\upsilon_m^1 \rightarrow c_m^1$). The RBM bands of both semiconducting and metallic tubes seem to show simultaneous intensity attenuation due to electrochemical charging. The spectra in Figure 10 also display the bands of acetonitrile at 380 and 1375 cm^{-1} (δC−C≡N and δC−H). These acetonitrile bands can serve as internal reference for calibration of Raman frequency and intensity. The occurrence of narrow metallic tubes in CO-SWCNTs manifests itself by the TM band, which shows a shape characteristic for the Breit−Wigner−Fano (BFW) broadening.

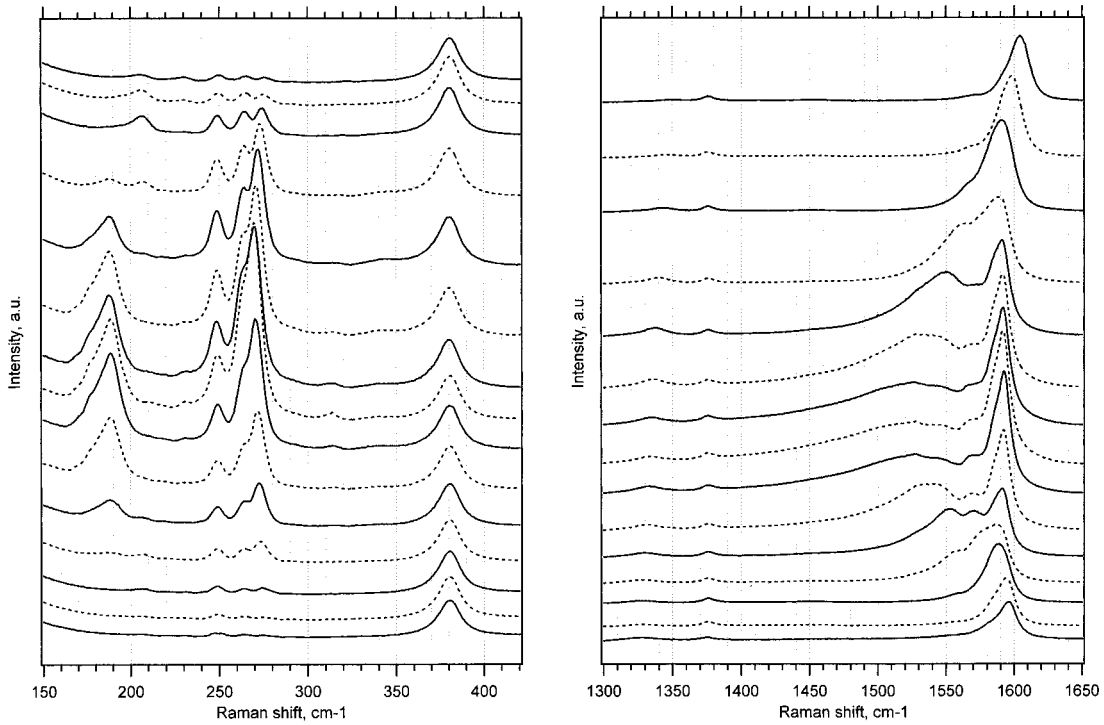

Figure 10. CO-SWCNT: In-situ Raman spectra in 0.2 M $LiClO_4$ + acetonitrile excited at $\lambda = 514.5$ nm. The applied potential was (in V vs Ag/AgCl) 1.4, 1.2, 1.0, 0.8, 0.6, 0.4, 0.2, 0, −0.2, −0.4, −0.6, −0.8, −1.0, −1.2, −1.4 for curves from top to bottom. The spectra are offset for clarity, but the intensity scale is identical for all plots in the given spectral region.

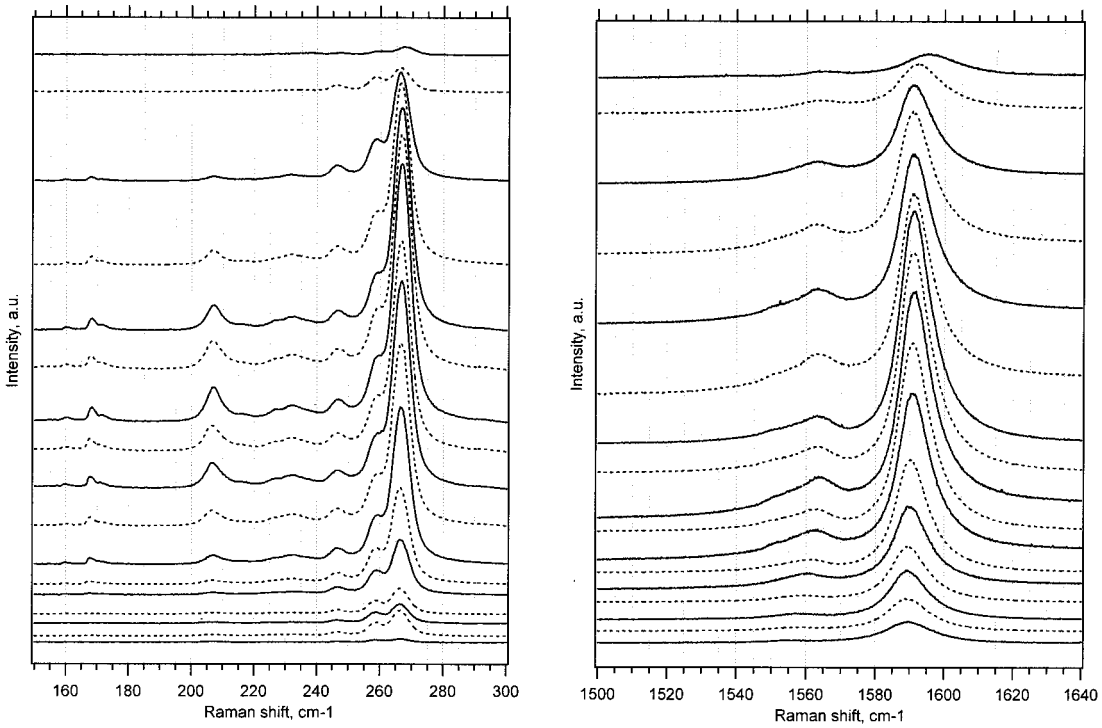

Figure 11. CO-SWCNT: In-situ Raman spectra in 0.2 M $LiClO_4$ + acetonitrile excited at $\lambda = 754.0$ nm. The applied potential was (in V vs Ag/AgCl) 1.4, 1.2, 1.0, 0.8, 0.6, 0.4, 0.2, 0, −0.2, −0.4, −0.6, −0.8, −1.0, −1.2, −1.4, −1.5, −1.6 for curves from top to bottom. The spectra are offset for clarity, but the intensity scale is identical for all plots in the given spectral region.

The BWF broadening is removed when the CO-SWCNTs are excited at $\lambda = 754$ nm (Figure 11). This fits the fact that the spectrum in Figure 11 is dominated by semiconducting tubes (250−270 cm^{-1}), which are in resonance with the $v_s^2 \rightarrow c_s^2$ transition. (The other corresponding transition, $v_s^1 \rightarrow c_s^1$ of CO-SWCNTs is shown on Figure 3. Apparently, the narrow semiconducting tubes in CO-SWCNTs exhibit similar signatures in NIR (Figure 3) and Raman (Figure 11) spectra.) The multiline feature of high-frequency RBM occurs at both excitation wavelengths used (Figures 10 and 11), which indicates that CO-SWCNTs contain a polydisperse mixture of narrow tubes ($d <$ 1 nm) that are both metallic and semiconducting. Figure 11 displays also a weak signal of wide metallic tubes (167 and 207 cm^{-1}), which resonate with the $v_m^1 \rightarrow c_m^1$ transition.

Figure 12 plots the relative intensity changes of RBM in CO-SWCNTs excited at $\lambda = 514.5$ nm. The plot presumably reflects a convolution of doping-driven changes in resonance enhancement with the concentration of individual tube diameters. Qualitatively, we see the expected symmetrical intensity attenuation upon anodic and cathodic charging.[12] Also we may see the marked relations to electronic spectra (Figure 4).

Conclusions

Electrochemistry of SWCNTs in dry and oxygen-free solutions of $LiClO_4$ + acetonitrile is controlled by capacitive charging. Faradaic pseudocapacitance of surface oxides is promoted by trace water. The cathodic voltammetric peak at ca. −0.6 to −0.7 V is assigned to this effect; an alternative interpretation based on Li^+ insertion seems to be less supported.

Electrochemical charging of SWCNTs in acetonitrile electrolyte solution allows easy and precise control of the population of electronic states, which occur at energies between about ± 1.2 eV vs the Fermi level. This can be traced via reversible bleaching of the electronic transitions between Van Hove singularities in the vis-NIR region. The potential-controlled optical switching of SWCNTs occurs within subsecond times.

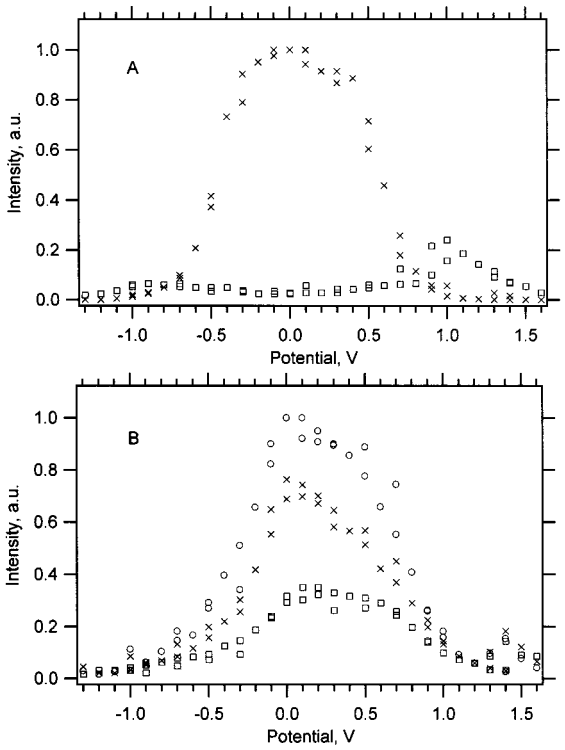

Figure 12. CO-SWCNT: Raman intensity of RBM at 185 cm^{-1} (×) or 205 cm^{-1} (□), respectively (plot A), and 245 cm^{-1} (□), 265 cm^{-1} (×) or 270 cm^{-1} (○), respectively (plot B).

An aprotic medium offers a broader electrochemical window for tuning of electronic properties of SWCNTs, compared to an aqueous electrolyte solution. Nevertheless, SWCNTs are sensitive to photoelectrochemical oxidative breakdown at potentials larger than ca. 1.2 V. A simultaneous application of the laser light and anodic polarization is essential for burning

of SWCNTs. No breakdown of SWCNTs occurred if the laser excitation and the anodic potential (>1.2 V) were not applied simultaneously. The SWCNT are also photoelectrochemically unstable at potentials negative to ca. −1.2 V.

Electrochemical tuning of the population of electronic states of SWCNTs can also be easily detected by resonance Raman scattering. Reversible changes of intensity and frequency of the Raman spectra can be monitored even during cyclic voltammetry at low scan rates.

The vis-NIR spectroelectrochemistry and Raman spectra excited at various photon energies and various potentials give a complex picture of a SWCNT sample. In particular, the potential-dependent quenching of vis-NIR and Raman spectra is a useful tool to the analysis of tubes of varying diameter and helicity.

Acknowledgment. Financial support from IFW-Dresden, Grant Agency of the Czech Republic (L.K., contract No. 203/99/1015) and Humboldt Foundation (P.R.) is gratefully acknowledged. Richard Jirasek (J. Heyrovsky Institute) contributed with electrochemical and quartz microbalance measurements.

References and Notes

(1) Rajalakshmi, N.; Dhathathreyan, K. S.; Govindaraj, A. *Electrochim. Acta* **2000**, *45*, 4511.

(2) Nützenadel, C.; Züttel, A.; Chartouni, D.; Schlapbach, L. *Electrochem. Solid-State Lett.* **1999**, *2*, 30.

(3) Claye, A. S.; Fischer, J. E.; Huffman, C. B.; Rinzler, A. G.; Smalley, R. E. *J. Electrochem. Soc.* **2000**, *147*, 2845.

(4) Frackowiak, E.; Beguin, F. *Carbon* **2001**, *39*, 937.

(5) Barisci, J. N.; Wallace, G. G.; Baughman, R. H. *J. Electroanal. Chem.* **2000**, *488*, 92.

(6) Ma, R. Z.; Liang, J.; Wei, B. Q.; Zhang, B.; Xu, C. L.; Wu, D. H. *J. Power Sources* **1999**, *84*, 126.

(7) Liu, C.; Bard, A. J.; Wudl, F.; Weitz, I.; Heath, J. R. *Electrochem. Solid-State Lett.* **1999**, *2*, 577.

(8) Niu, C.; Sichel, E. K.; Hoch, R.; Moy, D.; Tennent, H. *Appl. Phys. Lett.* **1997**, *70*, 1480.

(9) Liu, C.; Fan, Y. Y.; Liu, M.; Cong, H. T.; Cheng, H. M.; Dresselhaus, M. S. *Science* **1999**, *286*, 1127.

(10) Barisci, J. N.; Wallace, G. G.; Baughman, R. H. *Electrochim. Acta* **2000**, *46*, 509.

(11) Barisci, J. N.; Wallace, G. G.; Baughman, R. H. *J. Electrochem. Soc.* **2000**, *147*, 4580.

(12) Kavan, L.; Rapta, P.; Dunsch, L. *Chem. Phys. Lett.* **2000**, *328*, 363.

(13) Alvarez, L.; Righi, A.; Guillard, T.; Rols, S.; Anglaret, E.; Laplaze, D.; Sauvajol, J. L. *Chem. Phys. Lett.* **2000**, *316*, 186.

(14) Kataura, H.; Kumayawa, Y.; Maniwa, Y.; Umezu, I.; Suzuki, S.; Ohtsuka, Y.; Achiba, Y. *Synth. Met.* **1999**, *103*, 2555.

(15) Jacquemin, R.; Kazaoui, S.; Yu, D.; Hassanien, A.; Minami, N.; Kataura, H.; Achiba, Y. *Synth. Met.* **2000**, *115*, 283.

(16) Petit, P.; Mathis, C.; Journet, C.; Bernier, P. *Chem. Phys. Lett.* **1999**, *305*, 370.

(17) Rao, A. M.; Eklund, P. C.; Bandow, S.; Thess, A.; Smalley, R. E. *Nature* **1997**, *388*, 257.

(18) Kazaoui, S.; Minami, N.; Jacquemin, R.; Kataura, H.; Achiba, Y. *Phys. Rev. B* **1999**, *60*, 13339.

(19) Jouguelet, E.; Mathis, C.; Petit, P. *Chem. Phys. Lett.* **2000**, *318*, 561.

(20) Claye, A.; Rahman, S.; Fischer, J. E.; Sirenko, A.; Sumanasekera, G. U.; Eklund, P. C. *Chem. Phys. Lett.* **2001**, *333*, 16.

(21) Nikolaev, P.; Bronikowski, M. J.; Bradley, R. K.; Rohmund, F.; Colbert, D. T.; Smith, K. A.; Smalley, R. E. *Chem. Phys. Lett.* **1999**, *313*, 91.

(22) Bronikowski, M. J.; Willis, P. A.; Colbert, D. T.; Smith, K. A.; Smalley, R. E. *J. Vac. Sci. Technol. A* **2001**, *19*, 1800.

(23) Jost, O.; Gorbunov, A. A.; Pompe, W.; Pichler, T.; Friedlein, R.; Knupfer, M.; Reibold, M.; Bauer, M.; Dunsch, L.; Golden, M. S. *Appl. Phys. Lett.* **1999**, *75*, 2217.

(24) Kazaoui, S.; Minami, N.; Kataura, H.; Achiba, Y. *Synth. Met.* **2001**, *121*, 1201.

(25) Milnera, M.; Kürti, J.; Hulman, M.; Kuzmany, H. *Phys. Rev. Lett.* **2000**, *84*, 1324.

(26) Sumanasekera, G. U.; Allen, J. L.; Fang, S. L.; Loper, A. L.; Rao, A. M.; Eklund, P. C. *J. Phys. Chem. B* **1999**, *103*, 4292.

(27) Panitz, J. C.; Joho, F.; Novák, P. *Appl. Spectrosc.* **1999**, *53*, 1199

(28) Huang, W.; Frech, R. *J. Electrochem. Soc.* **1998**, *145*, 765.

(29) Inaba, M.; Yoshida, H.; Ogumi, Z.; Abe, T.; Mizutani, Y.; Asano, M. *J. Electrochem. Soc.* **1995**, *142*, 20.